

# Beyond the Golden Data: Resolving the Motion-Vision Quality Dilemma via Timestep Selective Training

Xiangyang Luo<sup>1,2\*</sup> Qingyu Li<sup>2†</sup> Yuming Li<sup>2</sup> Guanbo Huang<sup>1</sup> Yongjie Zhu<sup>2</sup>  
 Wenyu Qin<sup>2</sup> Meng Wang<sup>2</sup> Pengfei Wan<sup>2</sup> Shao-Lun Huang<sup>1†</sup>  
<sup>1</sup>Tsinghua University <sup>2</sup>Kling Team, Kuaishou Technology

## Abstract

Recent advances in video generation models have achieved impressive results. However, these models heavily rely on the use of high-quality data that combines both high visual quality and high motion quality. In this paper, we identify a key challenge in video data curation: the Motion-Vision Quality Dilemma. We discovered that visual quality and motion intensity inherently exhibit a negative correlation, making it hard to obtain golden data that excels in both aspects. To address this challenge, we first examine the hierarchical learning dynamics of video diffusion models and conduct gradient-based analysis on quality-degraded samples. We discover that quality-imbalanced data can produce gradients similar to golden data at appropriate timesteps. Based on this, we introduce the novel concept of Timestep selection in Training Process. We propose Timestep-aware Quality Decoupling (TQD), which modifies the data sampling distribution to better match the model’s learning process. For certain types of data, the sampling distribution is skewed toward higher timesteps for motion-rich data, while high visual quality data is more likely to be sampled during lower timesteps. Through extensive experiments, we demonstrate that TQD enables training exclusively on separated imbalanced data to achieve performance surpassing conventional training with better data, challenging the necessity of perfect data in video generation. Moreover, our method also boosts model performance when trained on high-quality data, showcasing its effectiveness across different data scenarios.

## 1. Introduction

Recent advancements in video generation models [3, 13, 14, 22, 39] have made impressive strides in the field of Artificial Intelligence Generated Content. Video generation mod-

\* This work was conducted during the author’s internship at Kling Team, Kuaishou Technology.

† Corresponding authors.

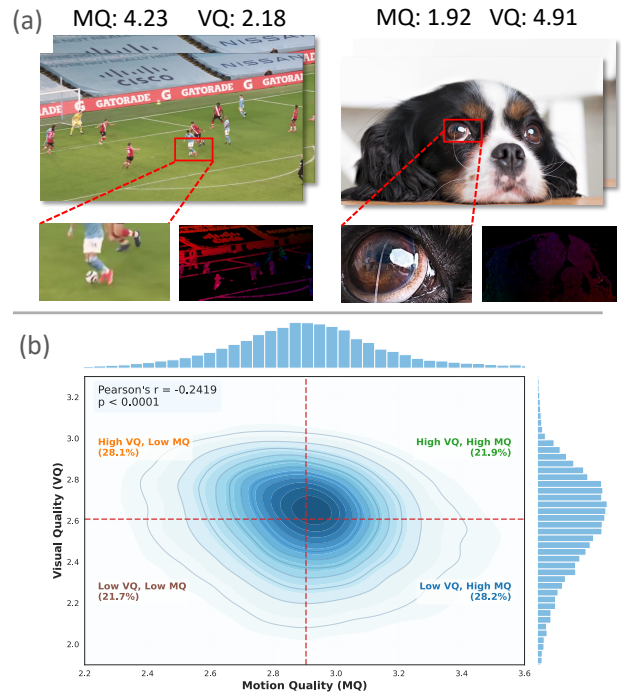


Figure 1. The motion-vision dilemma in video data. (a) Illustrates two cases: a high-MQ, low-VQ action scene (left) and a low-MQ, high-VQ static scene (right), with their corresponding optical flow maps below visualizing the difference in motion intensity. (b) The 2D density plot over Koala36M dataset confirms this trade-off. MQ and VQ exhibit a negative correlation, with the majority of samples (56.3% total) falling into the high-VQ/low-MQ or low-VQ/high-MQ quadrants, as defined by the median lines. Data with both high qualities is less common (21.9%).

els are capable of producing high-quality, coherent videos, with applications spanning entertainment [12, 27, 29, 30, 42], advertising [7, 44], and education [16, 28]. These models, however, heavily depend on high-quality training data—specifically, golden data that combines both high vision quality (VQ) and high motion quality (MQ). Unfortunately, such datasets are rare and expensive to obtain, which

presents a major limitation in scaling these models.

Most existing works address this issue from the data selection perspective [4, 19, 39]. Large video datasets are first collected and then filtered using strict criteria to retain only samples that satisfy both high VQ and high MQ. For instance, videos with minor blur or irregular motion are typically filtered out, even though they may still contain valuable learning signals for either visual or motion representation. While this filtering improves training data quality, it also removes a substantial portion of potentially useful videos, leading to significant data waste and a dataset biased toward perfect samples.

To better understand the scarcity of such dual-quality data, we analyzed the Koala36M dataset [41] and visualized the relationship between VQ and MQ, as shown in Figure 1. Figure 1(a) presents two representative imperfect cases: a high-MQ but low-VQ action scene (left) and a high-VQ but low-MQ static scene (right), with corresponding optical-flow visualizations highlighting their motion intensity differences. Figure 1(b) further depicts the distribution of all samples, revealing a clear negative correlation between motion and visual quality ( $r = -0.2419$ ). Only 21.9% of videos fall into the quadrant with both high VQ and MQ (defined by median lines; practical filtering would use much higher thresholds), confirming that the golden data emphasized by prior data-selection pipelines is statistically rare. We refer to this inherent conflict between motion and visual fidelity as the Motion-Vision Quality Dilemma.

In this work, we take a different perspective—shifting the question from which videos should be kept to how can we use imperfect videos more effectively? We begin by analyzing the learning behavior of video diffusion models and make two key observations. First, the denoising process exhibits hierarchical learning: motion emerges at high-noise timesteps while details refine at low-noise timesteps. Second, and more critically, through gradient-based analysis we discover that quality-imbalanced samples can match golden data’s gradients at appropriate timesteps. This reveals that imbalanced data need not be discarded but should be strategically allocated to matching denoising phases where they provide equivalent learning signals. Building upon this observation, we propose timestep selection in the training process and instantiate it through Timestep-aware Quality Decoupling. Instead of sampling timesteps equally across all data, we adjust the sampling distribution based on each video’s quality profile. High-MQ videos are biased toward higher-noise timesteps, whereas high-VQ videos are biased toward lower-noise timesteps. This design allows the model to leverage imperfect data effectively, aligning each sample with the phase of diffusion training where it provides the most benefit.

Extensive experiments demonstrate that TQD enables training exclusively on separated imbalanced

data—containing only high-VQ/low-MQ or high-MQ/low-VQ samples—to achieve performance surpassing conventional timestep sampling trained on datasets with golden data, challenging the necessity of dual-quality samples in video generation. Moreover, TQD further boosts model performance when applied to high-quality data, showcasing its effectiveness and robustness across diverse data scenarios. These results open a more data-efficient and scalable path for video generation. The key contributions of this paper are as follows:

- We identify and define the Motion-Vision Quality Dilemma in video generation.
- We conduct gradient analysis revealing that quality-imbalanced data can produce learning signals equivalent to golden data at appropriate timesteps, providing theoretical foundation for timestep-selective training.
- We introduce and implement Timestep-Selective Training and propose the Timestep-aware Quality Decoupling (TQD) framework for video diffusion models.
- We empirically demonstrate that TQD allows training with imbalanced data to achieve performance surpassing conventional training method, validating the effectiveness of this new paradigm.

## 2. Related Work

### 2.1. Video Diffusion Models

Recent progress in video generation is largely driven by video diffusion models [3, 13, 14, 22, 36, 38, 39, 46], which synthesize videos by progressively denoising Gaussian noise into coherent temporal sequences. Early approaches [3, 13] factorized spatial and temporal modeling through separated attention mechanisms—applying spatial self-attention within frames followed by temporal attention across frames. This decomposition enables efficient training by leveraging pretrained image models [1, 6, 34], but the separated treatment of space and time can cause temporal artifacts and inconsistent motion. Recent architectures [22, 33, 46] have shifted toward unified 3D attention that jointly models spatiotemporal correlations, naturally capturing space-time dependencies and achieving better motion coherence, though at higher computational cost.

The training formulation has also evolved beyond the classical diffusion objective [17], which learns to predict noise  $\epsilon_\theta(x_t, t)$  by minimizing  $\mathcal{L}_{\text{diff}} = \mathbb{E}[\|\epsilon - \epsilon_\theta(x_t, t)\|^2]$ , where  $x_t = \sqrt{\bar{\alpha}_t}x_0 + \sqrt{1 - \bar{\alpha}_t}\epsilon$ . While this stochastic denoising excels at spatial fidelity, recent frameworks [22, 24, 39] adopt flow matching [25], which deterministically transports samples from noise to data by learning a velocity field:  $\frac{dx_t}{dt} = v_\theta(x_t, t)$ . This ODE-based formulation directly models probability flow, favoring temporally stable trajectories and smoother motion. Despite these advances, existing methods all assume high-quality data with both ex-

cellent visual and motion quality. Our work addresses the practical challenge of quality imbalance, demonstrating that principled timestep-aware training effectively leverages imperfect data and achieves consistent improvements across both diffusion and flow matching paradigms.

## 2.2. Data Selection and Curation

Data curation plays an important role in large-scale generative modeling. In vision-language modeling, both curated datasets [35] and recent model-driven selection approaches [11, 23, 32, 43] show that selecting informative examples under limited compute can significantly improve generalization. In diffusion models, explicit data-centric work is more limited. D2C [19] condenses training sets via difficulty scoring; FiFA [45] filters preference data based on informativeness; and Alchemist [37] upgrades noisy public text-to-image data through iterative filtering. Mild corruption applied to pre-training data has also been shown to improve robustness [5]. Works like Ambient Diffusion [10] further demonstrate training on uncurated, bad data yields robust models but limited in image generation. For video generation, recent systems [22, 39] adopt multi-stage filtering pipelines evaluating visual quality, motion consistency, and caption alignment. Yet these pipelines discard videos whenever either VQ or MQ is low, meaning that samples strong in only one dimension are never exploited. In contrast, our approach explicitly leverages such imbalanced data by routing high-MQ/low-VQ and high-VQ/low-MQ videos to different regions of the denoising process, reducing reliance on rare jointly high-quality video samples.

## 2.3. Timestep and Loss Reweighting

Diffusion models learn across a sequence of noise levels, and many works redesign timestep sampling or loss weighting to improve training. Foundational improvements such as cosine schedules [31] and SNR-based loss reweighting [15] highlight that different timesteps contribute unequally to optimization. Perception Prioritized training [8] further adjusts weights to favor perceptually important denoising stages, while curriculum-based strategies [21] gradually expand the range of timesteps used during training to improve stability. However, these approaches apply a uniform timetable to all training samples: each image or video receives the same per-timestep weighting regardless of its content. Existing methods therefore optimize when the model should learn, but not what type of data should be emphasized at each timestep. Our TQD method differs by conditioning timestep allocation on sample-specific quality indicators, exploiting the natural hierarchy that early timesteps primarily shape motion while later timesteps refine appearance. This enables effective learning from imperfect data—something existing timestep curricula cannot address.

## 3. Method

### 3.1. The Vision-Motion Quality Dilemma

We employ the VideoAlign [26] framework to score a random sampled subset of the Koala-36M dataset [41]. Since the original VideoAlign is trained on generated videos, we retrain the model on real-world videos to better suit our analysis of natural video distributions. We then plot the distribution of MQ and VQ scores. As illustrated in Fig. 1(b), we divide the data into four quadrants based on the median values of the collected data for analysis purposes (note that practical filtering pipelines would use much higher thresholds). Notably, data satisfying both high VQ and high MQ (above median) accounts for only 21.9%, while high-VQ/low-MQ and high-MQ/low-VQ data each comprise around 28%. This reveals a clear pattern: data excelling in both metrics is less common than data showing strength in one metric while being weak in the other.

In addition, we compute the Pearson correlation coefficient between VQ and MQ as  $-0.2187$ , with a  $p$ -value  $< 0.001$ , indicating a trade-off between VQ and MQ. We term this phenomenon the Motion-Vision Quality Dilemma, which contributes to the scarcity of golden data with high quality in both metrics. Through this analysis, we highlight that while golden data is sparse, there exist large amounts of data that excel in only one metric (either VQ or MQ, but not both). Conventional filtering pipelines [22, 39] discard these, yet our timestep selection framework demonstrates their utility in training effective video diffusion models.

### 3.2. Quality Dynamics Analysis in Video Diffusion Process

Prior work has shown that image diffusion models determine layout in early timesteps and refine details in later ones [40]. Building upon this insight, we investigate its extension to video diffusion models and empirically verify that they prioritize motion information in early timesteps and visual details in later ones. As depicted in Fig. 2(a), visualizing the video generation process demonstrates that layout and motion are established early, with content refined subsequently.

Furthermore, to demonstrate that imbalanced data can provide gains comparable to golden data at specific timesteps, we conduct a gradient-based analysis across 120 samples with three types of VQ degradation (blur, compression, noise; 40 each) and MQ degradation (frame shuffling). For each degraded sample, we compute gradients of a video diffusion model [39] at various timesteps and measure the L2 distance to gradients from the original sample, averaging across all samples. As shown in Fig. 2(b), VQ degradation maintains gradient similarity with the original at high timesteps (high noise levels), suggesting that high-MQ/low-VQ data effectively supports motion learning in early de-

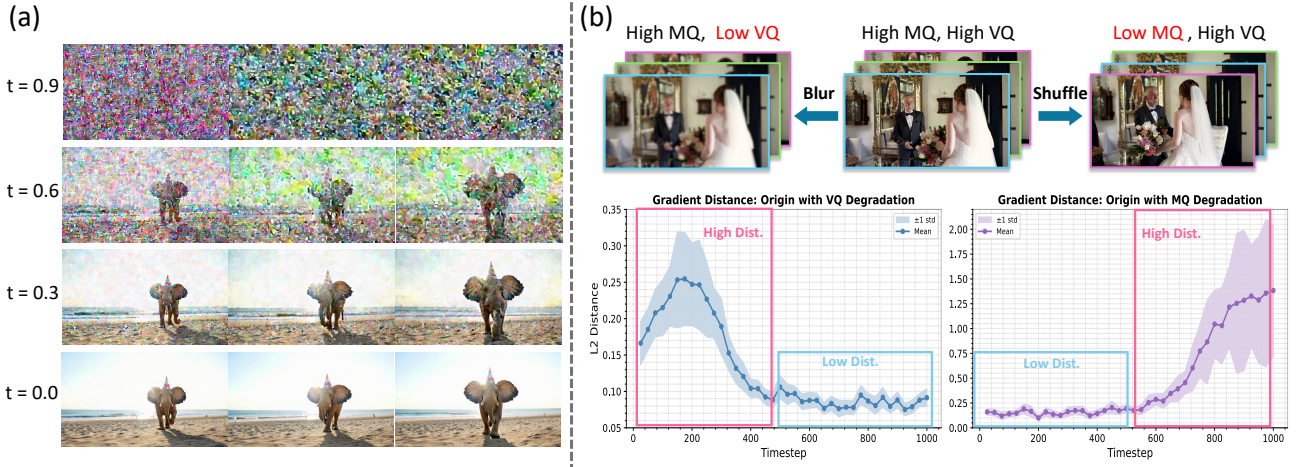


Figure 2. (a) Video diffusion models exhibit hierarchical denoising: high-noise stages ( $t = 0.9, 0.6$ ) establish motion and composition, while low-noise stages ( $t = 0.3, 0.0$ ) refine details and textures. (b) Gradient analysis under quality degradations, averaged over 120 samples with three VQ degradation types (blur, compression, noise) and MQ degradation (shuffle). VQ degradation aligns with the original at high timesteps, while MQ degradation aligns at low timesteps, revealing that quality-imbalanced samples can match golden data’s gradients at appropriate timesteps and should be strategically allocated across the denoising process.

noising stages. Conversely, MQ degradation preserves gradient similarity at low timesteps (low noise levels), indicating that high-VQ/low-MQ data contributes meaningfully to detail refinement in later stages. These complementary patterns motivate our timestep-aware training strategy: samples with high VQ can be effectively utilized at lower timesteps, while samples with high MQ contribute meaningfully at higher timesteps, enabling efficient exploitation of data with varying quality characteristics.

### 3.3. Timestep-Selective Training with TQD

Based on the analysis in Sec. 3.2, we propose Timestep-aware Quality Decoupling (TQD), a data-aware timestep selection training method that adaptively adjusts sampling strategies for each individual sample. Unlike conventional video generation models that apply uniform or logit-normal timestep sampling equally across all samples, TQD adapts the timestep sampling to each sample’s quality characteristics through a two-level adaptive mechanism: (1) sample-level weighting based on absolute quality to down-weight samples lacking distinctive strengths in either dimension, and (2) timestep-level distribution adjustment based on relative quality to match specialized data to appropriate denoising stages. The overall method is shown in Fig. 3.

We precompute VQ and MQ scores for each sample in the training dataset, and normalize them to  $vq_{\text{norm}}, mq_{\text{norm}} \in [0, 1]$  via min-max normalization. These normalized scores serve as the foundation for both sample-level and timestep-level adaptation.

**Sample-Level Weighting via Absolute Quality.** To filter low-quality samples where both motion and visual quality

are poor, we introduce a quality-based dropout mechanism. We use  $\max(vq_{\text{norm}}, mq_{\text{norm}})$  as an absolute quality indicator, representing the sample’s best attribute. During batch preparation, each sample is retained with probability:

$$p_{\text{sample}} = \max(vq_{\text{norm}}, mq_{\text{norm}}). \quad (1)$$

This weighting scheme ensures that samples with at least one distinctive quality (high MQ or high VQ) receive sufficient training emphasis, while suppressing samples lacking notable strengths in either dimension. Samples with both low MQ and low VQ are naturally down-weighted, preventing them from dominating the training despite having small relative quality differences.

**Timestep-Level Distribution Adjustment via Relative Quality.** For retained samples, we adaptively adjust their timestep sampling distribution based on the relative quality difference between motion and visual attributes. We parameterize the timestep distribution as a quality-dependent Beta distribution over the normalized interval  $[0, 1]$ :

$$p(t|x_0) \propto \text{Beta}(t; \mu(x_0) \times \kappa(x_0), (1 - \mu(x_0)) \times \kappa(x_0)), \quad (2)$$

where  $t \in [0, 1]$  denotes the normalized timestep and  $x_0$  represents the data sample. The Beta distribution is characterized by two sample-dependent parameters: the center  $\mu(x_0)$  and the concentration  $\kappa(x_0)$ , which are dynamically computed from the sample’s quality metrics.

The sampling center  $\mu$  captures the relative strength between motion and visual quality:

$$\mu = 0.5 + 0.5 \times (mq_{\text{norm}} - vq_{\text{norm}}), \quad (3)$$

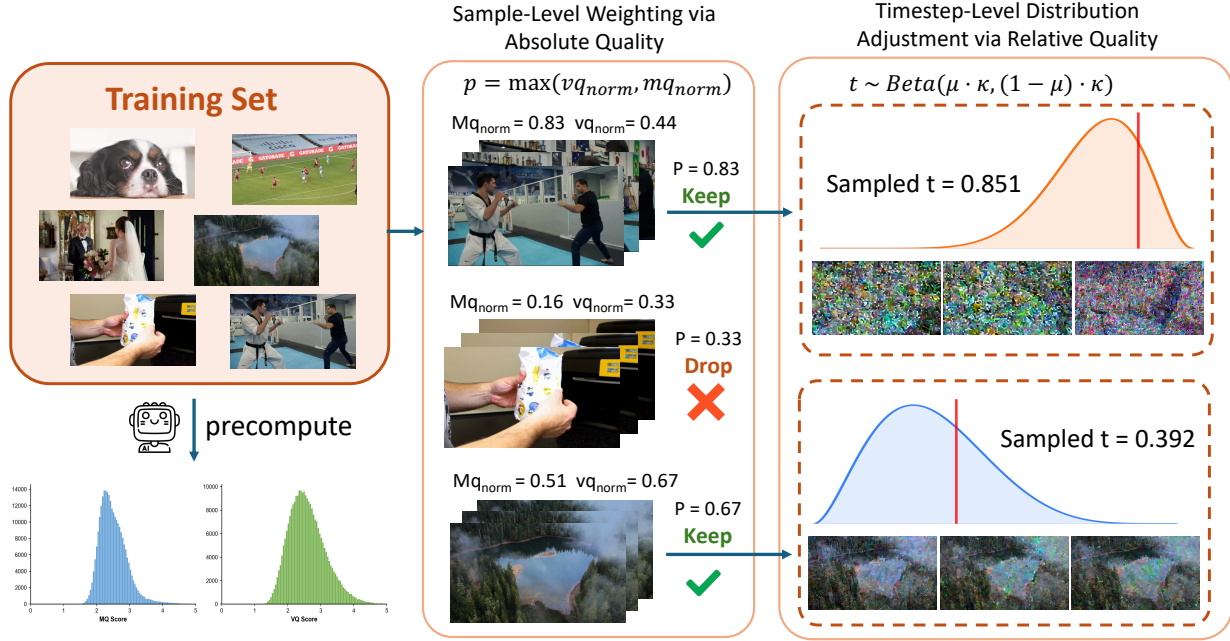


Figure 3. Overview of our timestep selective training process. Given bimodal quality distributions in training data (left), TQD employs quality-based sample dropout (middle) and adaptive timestep sampling via Beta distributions (right). Samples with high motion intensity are directed toward large timesteps, those with high visual quality toward small timesteps, achieving specialized learning across denoising process.

where  $(mq_{\text{norm}} - vq_{\text{norm}}) \in [-1, 1]$  reflects the comparative advantage. Samples with high MQ relative to VQ ( $\mu > 0.5$ ) shift the distribution toward higher timesteps, focusing on motion learning during early denoising stages. Conversely, samples with high VQ relative to MQ ( $\mu < 0.5$ ) bias toward lower timesteps, emphasizing appearance details in later refinement stages.

The concentration parameter  $\kappa$  controls the distribution’s peakedness based on the quality disparity:

$$\kappa = \kappa_{\text{base}} + (\kappa_{\text{max}} - \kappa_{\text{base}}) \times |mq_{\text{norm}} - vq_{\text{norm}}|, \quad (4)$$

where  $|mq_{\text{norm}} - vq_{\text{norm}}| \in [0, 1]$  quantifies the quality imbalance. A larger disparity produces a higher  $\kappa$ , yielding a more peaked distribution around  $\mu$ , thus providing stronger timestep specialization for imbalanced samples. For balanced samples (golden data with high MQ and VQ, or low-quality data already filtered by sample-level weighting), the distribution becomes flatter and approaches the baseline sampling. The base concentration  $\kappa_{\text{base}}$  is set to match the original training scheme:  $\kappa_{\text{base}} = 2$  for uniform timestep sampling (equivalent to  $\text{Beta}(1, 1)$ ), or  $\kappa_{\text{base}} = 4$  to approximate logit-normal distributions. This design ensures that when  $mq_{\text{norm}} = vq_{\text{norm}}$ , our method degenerates to the standard sampling strategy.

**Combined Quality-Weighted Distribution.** Combining both sample-level and timestep-level mechanisms, the com-

plete quality-weighted timestep distribution becomes:

$$p(t) \propto \max(vq_{\text{norm}}, mq_{\text{norm}}) \cdot \text{Beta}(t; \mu \times \kappa, (1 - \mu) \times \kappa). \quad (5)$$

This formulation ensures that: (1) low-quality samples (LMLV) are down-weighted through the absolute quality term, (2) motion-specialized samples (HMLV) concentrate on large timesteps, (3) visual-specialized samples (LMHV) concentrate on small timesteps, and (4) golden samples (HMHV) maintain balanced timestep coverage. We provide visualization examples of sample-specific timestep distributions in the Appendix for intuitive understanding.

**Training Algorithm.** Our complete training procedure is outlined in Alg. 1. The method operates in two stages: (1) batch preparation where samples are retained with probability  $\max(vq_{\text{norm}}, mq_{\text{norm}})$  (Lines 4-10), implementing absolute quality weighting, and (2) timestep sampling where retained samples draw timesteps from Beta distributions parameterized by their relative quality difference (Lines 12-16). This design effectively utilizes imbalanced data while filtering low-quality samples, achieving superior performance to models trained on curated data while expanding the usable training corpus.

---

**Algorithm 1** Timestep-Selective Training with TQD

---

**Require:** Dataset  $\mathcal{D}$  with precomputed  $\{\text{vq}, \text{mq}\}$ , concentrations  $\kappa_{\text{base}}, \kappa_{\text{max}}$

- 1: Normalize  $\{\text{mq}, \text{vq}\}$  to  $[0, 1]$  for all  $x_0 \in \mathcal{D}$
- 2: // *Sample-level weighting via absolute quality*
- 3: **function** PREPAREBATCH( $\mathcal{D}$ , batch\_size)
- 4:    $\mathcal{B} \leftarrow \emptyset$
- 5:   **while**  $|\mathcal{B}| < \text{batch\_size}$  **do**
- 6:     Sample data  $x_0$  from  $\mathcal{D}$  with probability  $\frac{\max(\text{vq}_{\text{norm}}, \text{mq}_{\text{norm}})}{\text{Eq. (1)}}$
- 7:     Add  $x_0$  to  $\mathcal{B}$
- 8:   **end while**
- 9:   **return**  $\mathcal{B}$
- 10: **end function**
- 11: // *Timestep-level sampling via relative quality*
- 12: **while** not converged **do**
- 13:    $\mathcal{B} \leftarrow \text{PREPAREBATCH}(\mathcal{D}, \text{batch\_size})$
- 14:   **for each**  $x_0 \in \mathcal{B}$  **do**
- 15:     Compute  $\mu$  and  $\kappa$  ▷ Eq. (3) (4)
- 16:     Sample  $t \sim \text{Beta}(\mu\kappa, (1 - \mu)\kappa)$  ▷ Eq. (5)
- 17:     Sample  $x_1 \sim \mathcal{N}(0, I)$
- 18:     Compute  $x_t \leftarrow tx_1 + (1 - t)x_0$
- 19:   **end for**
- 20:   Update model:  $\mathcal{L} = \mathbb{E}_{x_0, x_1, t} [\|v_\theta(x_t, t, c) - (x_1 - x_0)\|^2]$
- 21: **end while**

---

## 4. Experiments

### 4.1. Implementation Details

#### 4.1.1. Model Setup

We conduct experiments on two high performance video diffusion models: CogVideoX-5B [46] and Wan-T2V-1.3B [39]. CogVideoX employs a standard diffusion process with uniform timestep sampling, while Wan-T2V utilizes flow matching with logit-normal timestep sampling. This diverse setup demonstrates the robustness of our method across different generative frameworks and sampling strategies.

#### 4.1.2. Dataset Setup

We curate a training set of 280K video-text pairs online for supervised fine-tuning. All samples are scored using VideoAlign [26] to obtain MQ and VQ metrics. The quality distribution is relatively balanced across the dataset. To analyze the effectiveness of our method under different quality regimes, we partition the data into four categories based on quality thresholds (MQ=2.5, VQ=2.7): High-MQ-High-VQ (HMHV, 100K samples), High-MQ-Low-VQ (HMLV, 80K samples), Low-MQ-High-VQ (LMHV, 80K samples), and Low-MQ-Low-VQ (LMLV, 30K samples). Detailed quality distributions are provided in the Appendix. Dense cap-

tions for all videos are generated using a vision-language model [9].

#### 4.1.3. Training Setup

We finetune Wan-T2V-1.3B with full parameter training using a batch size of 128, and fine-tune CogVideoX-5B with LoRA (rank=256) [18] using a batch size of 96. All models are trained for 2,000 steps from their respective base checkpoints. To comprehensively evaluate our method, we construct three training configurations: Set-A uses all four quality categories to simulate realistic data distributions commonly encountered in practice; Set-B uses only HMLV and LMHV samples to assess our method’s effectiveness under extreme quality imbalance where dual-quality data is completely absent; Set-C uses only HMHV samples to verify whether TQD provides additional gains even on rare golden data.

### 4.2. Quantitative Evaluation

We evaluate video generation quality using VBench [20] and VideoAlign [26]. Following standard practice, we use an LLM [9] to expand evaluation prompts into detailed descriptions matching our training data format. The baseline methods employ the default fine-tuning strategies for each model: uniform timestep sampling for CogVideoX and logit-normal sampling for Wan.

As shown in Table 1, TQD yields consistent gains across all data scenarios. Notably, under extreme quality imbalance (Set-B containing only HMLV and LMHV samples), TQD reaches or even surpasses results from naive fine-tuning on naturally distributed data—for example, Wan-T2V with TQD on Set-B (MQ: 2.1477, VQ: 3.2679) exceeds the baseline on Set-A (MQ: 2.1388, VQ: 3.2537). This shows that timestep-aware training can effectively exploit separated imperfect data and close, or even reverse, the gap with mixed-quality training. TQD also improves performance when trained solely on high-quality data (Set-C), demonstrating its robustness across different data regimes. We also observe smaller gains on CogVideoX, likely due to its LoRA-based fine-tuning setup, which constrains the model’s ability to fully adapt.

Interestingly, we also observe that fine-tuning with our curated dataset enhances downstream physical reasoning capabilities. We evaluate Wan 1.3B Set-A checkpoints on VideoPhy2 [2], specifically testing on hard cases that require understanding of physical dynamics. As shown in Table 2, TQD surpasses the baseline in both physical commonsense adherence and semantic alignment. To isolate TQD’s contribution from data filtering effects, we include a Data Filter Only variant that applies quality-based dropout without adaptive timestep allocation. TQD outperforms both, confirming that gains stem from timestep-aware routing rather than mere data selection.

Table 1. Quantitative comparison on VBench and VideoAlign metrics across different data settings. Best results in each setting are shown in **bold**.

Model	Setting	Method	VBench				VideoAlign	
			IQ	Aesthetic	Dynamic	MotionSmooth	MQ	VQ
Wan 1.3B	-	Basemodel	0.6935	0.5874	0.5938	0.9889	2.1993	3.3236
	Set-A	Baseline	0.6916	0.5722	0.5312	<b>0.9935</b>	2.1388	3.2537
		TQD	<b>0.7010</b>	<b>0.5757</b>	<b>0.6384</b>	0.9923	<b>2.2557</b>	<b>3.3450</b>
	Set-B	Baseline	0.6769	<b>0.5702</b>	0.5224	0.9923	2.0905	3.2338
		TQD	<b>0.6921</b>	0.5668	<b>0.5447</b>	<b>0.9935</b>	<b>2.1477</b>	<b>3.2679</b>
	Set-C	Baseline	0.6939	0.5798	0.5268	0.9920	2.1917	3.3378
		TQD	<b>0.7556</b>	<b>0.5847</b>	<b>0.6473</b>	<b>0.9931</b>	<b>2.2200</b>	<b>3.3743</b>
	CogVideoX 5B	-	Basemodel	0.6796	0.5361	0.7455	0.9780	2.2134
Set-A		Baseline	0.6811	<b>0.5388</b>	0.7500	<b>0.9781</b>	2.1855	<b>3.2593</b>
		TQD	<b>0.6816</b>	0.5386	<b>0.7723</b>	0.9780	<b>2.2345</b>	3.2570
Set-B		Baseline	0.6798	0.5379	0.7679	0.9781	2.1821	3.2407
		TQD	<b>0.6848</b>	<b>0.5381</b>	<b>0.7768</b>	<b>0.9793</b>	<b>2.2010</b>	<b>3.2499</b>
Set-C		Baseline	0.6814	0.5386	<b>0.7723</b>	0.9779	2.2028	3.2373
		TQD	<b>0.6857</b>	<b>0.5397</b>	0.7679	<b>0.9783</b>	<b>2.2448</b>	<b>3.2392</b>

Table 2. Quantitative comparison on Subject Alignment (SA) and Prompt Consistency (PC) metrics with VideoPhy2.

Model	SA $\uparrow$	PC $\uparrow$
Wan 1.3B	3.738	3.690
Baseline	3.786	3.709
Data Filter Only	3.795	3.756
TQD (Ours)	<b>3.820</b>	<b>3.843</b>

### 4.3. Qualitative Evaluation

Fig. 4 compares models trained on quality-imbalanced data from Set-B. Baseline training on such imbalanced data reveals quality degradation: visual artifacts such as hand distortions (top-left), motion incoherence failing to match prompt dynamics (top-right), and struggles with physical realism including unnatural foam dissipation and improper liquid spreading (bottom rows, red boxes). TQD effectively addresses these limitations by directing each sample to timesteps that match its quality strengths—motion-rich samples to high-noise stages, visually clean samples to low-noise stages. This yields videos with both visual fidelity and motion coherence, while notably improving physical plausibility in dynamics like foam dissipation and liquid flow, achieving quality on par with curated-data training.

### 4.4. Ablation Study

We conduct comprehensive ablation studies to validate our design choices. All experiments are performed on Wan 1.3B with Set-A.

**Component Analysis.** Table 3 dissects TQD’s two core components on Wan Set-A. Adaptive timestep allocation via Beta distributions brings substantial improvements by directing samples to their optimal denoising stages based on quality characteristics. Quality-based dropout further enhances performance by filtering low-quality samples and rebalancing the training distribution. Combining both mechanisms yields synergistic gains (+0.1169 MQ, +0.0913 VQ), demonstrating that sample-level filtering and timestep-level adaptation mutually reinforce each other to achieve superior video quality. MotionSmooth scores shows minimal and comparable variation across methods.

**Concentration Parameter.** The concentration parameter  $\kappa_{\max}$  controls the peakedness of timestep distributions—higher values create more concentrated distributions, with samples exhibiting larger MQ-VQ disparities receiving proportionally higher  $\kappa$  for stronger specialization. We set  $\kappa_{\text{base}} = 2$  for CogVideoX to match its baseline uniform sampling (Beta(1,1)), and  $\kappa_{\text{base}} = 4$  for Wan to approximate its logit-normal sampling. Table 4 systematically examines  $\kappa_{\max}$  across both architectures. We observe that CogVideoX achieves optimal performance at lower values, while Wan performs best at higher values. This difference

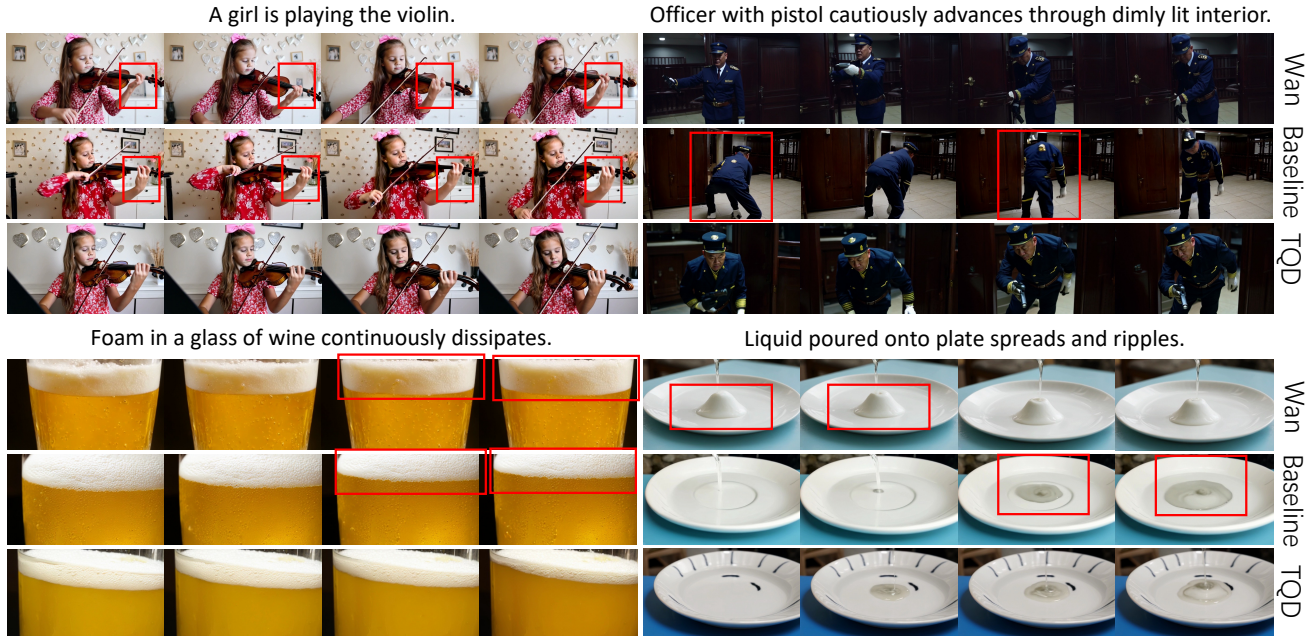


Figure 4. Qualitative comparison. TQD demonstrates superior performance across multiple quality dimensions. Top rows: improved visual quality with reduced hand distortion (left) and better motion coherence matching prompt dynamics (right). Bottom rows: enhanced physical plausibility in foam dissipation (left) and liquid dynamics (right), as highlighted in red boxes.

Table 3. Component ablation of TQD on Wan Set-A. We VBench metrics alongside VideoAlign scores to dissect motion-visual synergies.

Method	VBench				VideoAlign	
	IQ	Aesthetic	Dynamic	MotionSmooth	MQ	VQ
Baseline	0.6916	0.5722	0.5312	0.9935	2.1388	3.2537
+ Adaptive timestep	0.6972	0.5735	0.6340	<b>0.9937</b>	2.2193	3.3044
+ Quality dropout	0.6956	0.5701	0.5357	0.9916	2.1909	3.2921
+ Both (TQD)	<b>0.7010</b>	<b>0.5757</b>	<b>0.6384</b>	0.9923	<b>2.2557</b>	<b>3.3450</b>

suggests that models trained with uniform sampling may require more conservative distribution adjustments. Importantly, while  $\kappa_{\max}$  influences performance, all configurations of Wan substantially outperform their respective baselines (Wan baseline: MQ 2.1388, VQ 3.2537), demonstrating TQD’s robustness to this hyperparameter. Based on these findings, we adopt  $\kappa_{\max} = 20$  for CogVideoX and  $\kappa_{\max} = 30$  for Wan in all our experiments.

## 5. Conclusion

This paper identifies the Motion-Vision Quality Dilemma—a negative correlation between motion and visual quality that makes golden data statistically rare. Through gradient analysis, we reveal that quality-imbalanced samples can match golden data’s learning effectiveness at appropriate timesteps, motivating a shift from data filtering to timestep-aware training. We intro-

Table 4. Ablation study on concentration parameter  $\kappa_{\max}$  across CogVideoX and Wan architectures.

$\kappa_{\max}$	CogVideoX		Wan	
	MQ $\uparrow$	VQ $\uparrow$	MQ $\uparrow$	VQ $\uparrow$
10	2.2018	<b>3.2596</b>	2.2282	3.2808
20	<b>2.2345</b>	3.2570	2.2338	3.3020
30	2.2249	3.2543	<b>2.2557</b>	<b>3.3450</b>
40	2.2192	3.2535	2.2503	3.3152
50	2.2199	3.2504	2.2378	3.3089

duce Timestep-aware Quality Decoupling (TQD), which dynamically aligns each sample’s timestep distribution with its quality profile, achieving performance comparable to golden-data-only training with substantial gains on imbalanced datasets.

# Beyond the Golden Data: Resolving the Motion-Vision Quality Dilemma via Timestep Selective Training

## Supplementary Material

### 6. Timestep Distribution Analysis

Fig. 5 visualizes the timestep distributions across samples with different MQ and VQ scores under two  $\kappa_{\text{base}}$  configurations. We set  $\kappa_{\text{base}} = 2$  and 4 such that when  $\text{MQ} = \text{VQ}$ , the distributions degenerate to uniform and logit-normal, respectively. Notably, samples with higher MQ scores shift the distribution toward larger timesteps, while those with higher VQ scores concentrate sampling at lower timesteps. This adaptive reweighting allows our approach to dynamically allocate timesteps based on sample-specific quality metrics. However, samples with uniformly low or high MQ and VQ scores exhibit similar relative quality metrics, rendering timestep reweighting alone insufficient for differentiation. To complement this, we incorporate a probabilistic retention strategy during data loading, where each sample is kept with probability  $\max(\text{vq}_{\text{norm}}, \text{mq}_{\text{norm}})$  (see Sec. 3.3).

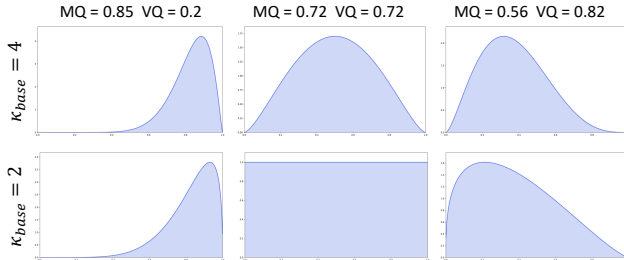


Figure 5. Timestep sampling distributions under varying quality scores. We visualize the Beta distributions with  $\kappa_{\text{base}} = 4$  (top) and  $\kappa_{\text{base}} = 2$  (bottom) for samples with different MQ and VQ scores. Left: High MQ, low VQ shifts toward large timesteps. Middle: Equal MQ and VQ yields centered distributions. Right: Low MQ, high VQ concentrates on small timesteps. Note that  $\kappa_{\text{base}} = 2$  degenerates to uniform when  $\text{MQ} = \text{VQ}$  (middle-bottom).

### 7. Computational Analysis

Our proposed training strategy requires VQ and MQ scores for each sample, which can be pre-computed offline before training begins. During training, we only perform two lightweight operations: sample dropout and timestep distribution computation based on VQ and MQ scores. The former seamlessly integrates with the dataloader’s prefetch mechanism, while the latter incurs negligible computational overhead. Consequently, our method achieves nearly identical GPU training time compared to the baseline, making it practically cost-free in terms of computational resources.

### 8. Dataset Settings

#### 8.1. Data Distribution Visualization

Fig. 6 illustrates the distribution of MQ and VQ scores across our 280K training samples, scored using VideoAlign [26]. The MQ distribution (left) exhibits clear bimodality with peaks at  $\approx 2.3$  and  $\approx 2.8$ , reflecting the natural divide between static and dynamic video content. In contrast, VQ distribution (right) follows a unimodal, right-skewed pattern centered at  $\approx 2.7$ , with most samples concentrated between 2.0–3.5. We partition this data into four subsets based on median-aligned thresholds ( $\text{MQ}=2.5$ ,  $\text{VQ}=2.7$ ): HMHV (100K), HMLV (80K), LMHV (80K), and LMLV (20K). Note that these distributions reflect our curated dataset where we deliberately selected different amounts from each quality category and mixed them together to ensure balanced training data.

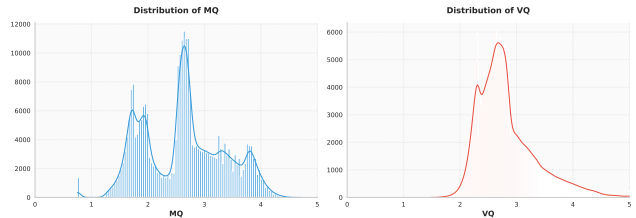


Figure 6. Data distribution of our collected training set.

#### 8.2. Video Caption Generation

To obtain precise and detailed video descriptions, we employ Gemini 2.5 Pro with carefully designed prompts that emphasize comprehensive scene analysis. Our prompting strategy instructs the model to provide structured captions covering eight key dimensions: (1) brief summary, (2) subject details including appearance and attire, (3) environment and context, (4) chronological actions and interactions, (5) aesthetic style, (6) technical visual attributes, (7) cinematography, and (8) camera movement. This structured approach ensures consistent, high-fidelity annotations that capture both visual content and stylistic nuances essential for training high-quality video generation models. Figure 7 illustrates our complete prompting template alongside a representative caption example generated for a wedding celebration scene.



You are an expert video analysis expert specializing in generating dense, high-fidelity captions for video datasets. Your goal is to describe the input video with extreme precision, focusing on visual details, action, and cinematographic attributes. Analyze the provided video and generate a caption that strictly follows the structure and style defined below. Your response must be a continuous text (or comprised of detailed segments) covering these specific aspects in order:

1. **Brief Summary:** A single sentence overview of the main subject and action.
2. **Subject Details:** Detailed description of the main character(s). Include age, ethnicity, hair, specific clothing details (colors, patterns, patches, layers), and initial pose/expression.
3. **Environment & Context:** Describe the background (wall colors, objects, furniture), lighting conditions (bright, dim, natural, artificial), and any inference about time of day or weather (or state if it's indeterminable).
5. **Chronological Action:** Describe the sequence of events. What is the subject doing? Who enters the frame? Describe movements from left to right or background to foreground. Focus on interactions and micro-expressions.
6. **Aesthetic Style:** Describe the visual style (e.g., realistic, cinematic, home video, TV series look). Mention the color palette (muted, vibrant, pastel).
7. **Technical Visuals:** Analyze the image quality terms: saturation (low/medium/high), contrast, lightness, and color tone (neutral, warm, cool).
8. **Cinematography:** Describe the movement of the camera.

# Style Guidelines

**Tone:** Objective, descriptive, and professional.

**Detail Level** Extremely high. Do not just say "a jacket," say "a black and white jacket with red accents and a patch on the left side."

**Format:** Do not use bullet points. Write in full, descriptive sentences.

A blonde woman in a white dress and a man in a patterned shirt embrace and congratulate a central male figure in a white t-shirt, culminating in the woman kissing him on the cheek during a celebratory event. The central subject is a young adult Caucasian male with short, light brown hair, wearing a plain white crew-neck t-shirt; his expression shifts from hearty laughter to a warm, appreciative smile. To his right stands a young adult Caucasian woman with blonde hair styled in a loose updo with strands framing her face, wearing long, dangling crystal earrings and a white dress with spaghetti straps and subtle beaded embellishments. To the left, another male subject appears, wearing a white short-sleeved button-down shirt featuring a dense blue floral or paisley pattern; he has short dark hair and is viewed primarily from the back and side. The scene takes place indoors against a textured, rustic wall that appears to be concrete or plaster with warm, earth-tone hues. In the blurred background, a figure sits behind a table with a laptop featuring a glowing logo, suggesting a DJ booth or reception setup. The lighting is artificial and atmospheric, with a strong backlight creating a halo effect on the woman's hair and a warm, ambient glow throughout the space.

The sequence begins with the central man laughing with his eyes nearly closed as he is embraced. The man in the patterned shirt enters fully from the left, wrapping his arms around the central man in a tight hug, turning his back to the camera. The woman stands close on the right, smiling broadly and looking affectionately at the central man, her hand resting near him. As the hug between the two men continues, the central man turns his head slightly toward the woman, locking eyes with her. The interaction concludes as the woman leans in and presses a kiss onto the central man's left cheek, causing him to smile widely while looking forward. The aesthetic style is that of high-end wedding videography, characterized by a candid, documentary feel that captures genuine emotion. The color palette is warm and inviting, dominated by creamy whites, skin tones, and the amber hues of the background lighting.

Visually, the footage exhibits high saturation, emphasizing the warmth of the scene, with a medium contrast that preserves details in the bright whites of the clothing and the darker shadows of the embrace. The lighting creates a soft, diffused look with a distinct warm color tone, enhancing the romantic and celebratory mood. The cinematography utilizes a static, medium close-up shot with a shallow depth of field, keeping the three subjects in sharp focus while blurring the background to isolate the intimate interaction. The camera remains steady, acting as an observer to the spontaneous affection without distracting movement.

Figure 7. Dense video captioning example. We leverage Gemini 2.5 Pro with structured prompts (top) to generate comprehensive video descriptions. The bottom panel shows an example caption (300+ words) for a wedding scene, demonstrating fine-grained descriptions of subjects' clothing, spatial dynamics, lighting, and camera techniques. This structured approach ensures annotation quality and consistency across our 280K training dataset.

## 9. More Qualitative Comparisons

Additional qualitative video comparisons are included in the supplementary materials, which further demonstrate the effectiveness of our approach.

## 10. Robustness to Scorer Noise

TQD employs probabilistic Beta-distribution sampling rather than hard-threshold filtering, providing inherent resilience to scorer noise—minor scoring errors only cause slight shifts in the sampling center ( $\mu$ ) without excluding any data. To quantify this, we inject 10% and 20% Gaussian noise into MQ and VQ scores on Wan Set-A.

As shown in Table 5, TQD with 20% noise still significantly outperforms the baseline across all metrics. This robustness is further validated by consistent improvements on the independent VBench metrics.

Table 5. Robustness to scorer noise on Wan Set-A. TQD maintains substantial gains over the baseline even with 20% noise.

Method	IQ	Aesthetic	Dynamic	Smooth	MQ	VQ
Uniform (no TQD)	0.6916	0.5722	0.5312	0.9935	2.1388	3.2537
TQD (0% noise)	<b>0.7010</b>	<b>0.5757</b>	<b>0.6384</b>	0.9923	<b>2.2557</b>	<b>3.3450</b>
TQD (10% noise)	0.6985	0.5743	0.6251	0.9931	2.2431	3.3285
TQD (20% noise)	0.6953	0.5731	0.6012	0.9928	2.2114	3.3085

## References

- [1] Stability AI. Stable diffusion, 2022. 2
- [2] Hritik Bansal, Clark Peng, Yonatan Bitton, Roman Goldenberg, Aditya Grover, and Kai-Wei Chang. Videophy-2: A challenging action-centric physical commonsense evaluation in video generation. *arXiv preprint arXiv:2503.06800*, 2025. 6
- [3] Andreas Blattmann, Tim Dockhorn, Sumith Kulal, Daniel Mendelevitch, Maciej Kilian, Dominik Lorenz, Yam Levi, Zion English, Vikram Voleti, Adam Letts, et al. Stable video diffusion: Scaling latent video diffusion models to large

- datasets. *arXiv preprint arXiv:2311.15127*, 2023. 1, 2
- [4] Rania Briq, Jiangtao Wang, and Stefan Kesselheim. Data pruning in generative diffusion models. *arXiv preprint arXiv:2411.12523*, 2024. 2
- [5] Hao Chen, Yujin Han, Diganta Misra, Xiang Li, Kai Hu, Difan Zou, Masashi Sugiyama, Jindong Wang, and Bhiksha Raj. Slight corruption in pre-training data makes better diffusion models. *Advances in neural information processing systems*, 37:126149–126206, 2024. 3
- [6] Junsong Chen, Jincheng Yu, Chongjian Ge, Lewei Yao, Enze Xie, Yue Wu, Zhongdao Wang, James Kwok, Ping Luo, Huchuan Lu, et al. Pixart- $\alpha$ : Fast training of diffusion transformer for photorealistic text-to-image synthesis. *arXiv preprint arXiv:2310.00426*, 2023. 2
- [7] Junhao Cheng, Yuying Ge, Yixiao Ge, Jing Liao, and Ying Shan. Animegamer: Infinite anime life simulation with next game state prediction. In *Proceedings of the IEEE/CVF International Conference on Computer Vision*, pages 10875–10885, 2025. 1
- [8] Jooyoung Choi, Jungbeom Lee, Chaehun Shin, Sungwon Kim, Hyunwoo Kim, and Sungroh Yoon. Perception prioritized training of diffusion models. *CoRR*, abs/2204.00227, 2022. 3
- [9] Gheorghe Comanici, Eric Bieber, Mike Schaekermann, Ice Pasupat, Noveen Sachdeva, Inderjit Dhillon, Marcel Blisstein, Ori Ram, Dan Zhang, Evan Rosen, et al. Gemini 2.5: Pushing the frontier with advanced reasoning, multimodality, long context, and next generation agentic capabilities. *arXiv preprint arXiv:2507.06261*, 2025. 6
- [10] Giannis Daras, Adrian Rodriguez-Munoz, Adam Klivans, Antonio Torralba, and Constantinos Daskalakis. Ambient diffusion omni: Training good models with bad data. *arXiv preprint arXiv:2506.10038*, 2025. 3
- [11] Benjamin Feuer, Jiawei Xu, Niv Cohen, Patrick Yubeaton, Govind Mittal, and Chinmay Hegde. SELECT: A large-scale benchmark of data curation strategies for image classification, 2024. 3
- [12] Xu Guo, Fulong Ye, Xinghui Li, Pengqi Tu, Pengze Zhang, Qichao Sun, Songtao Zhao, Xiangwang Hou, and Qian He. Dreamid-v: Bridging the image-to-video gap for high-fidelity face swapping via diffusion transformer. *arXiv preprint arXiv:2601.01425*, 2026. 1
- [13] Yuwei Guo, Ceyuan Yang, Anyi Rao, Zhengyang Liang, Yaohui Wang, Yu Qiao, Maneesh Agrawala, Dahua Lin, and Bo Dai. Animatediff: Animate your personalized text-to-image diffusion models without specific tuning. *arXiv preprint arXiv:2307.04725*, 2023. 1, 2
- [14] Yoav HaCohen, Nisan Chiprut, Benny Brazowski, Daniel Shalem, Dudu Moshe, Eitan Richardson, Eran Levin, Guy Shiran, Nir Zabari, Ori Gordon, et al. Ltx-video: Realtime video latent diffusion. *arXiv preprint arXiv:2501.00103*, 2024. 1, 2
- [15] Tiankai Hang, Shuyang Gu, Chen Li, Jianmin Bao, Dong Chen, Han Hu, Xin Geng, and Baining Guo. Efficient diffusion training via min-snr weighting strategy. In *Proceedings of the IEEE/CVF International Conference on Computer Vision (ICCV)*, pages 7441–7451, 2023. 3
- [16] Salma Hannouni, Sanaa El Filali, et al. Generative ai for education: A study of text-to-video generation for personalized learning. In *2025 International Conference on Circuit, Systems and Communication (ICCSC)*, pages 1–6. IEEE, 2025. 1
- [17] Jonathan Ho, Ajay Jain, and Pieter Abbeel. Denoising diffusion probabilistic models. *Advances in neural information processing systems*, 33:6840–6851, 2020. 2
- [18] Edward J Hu, Yelong Shen, Phillip Wallis, Zeyuan Allen-Zhu, Yuanzhi Li, Shean Wang, Lu Wang, Weizhu Chen, et al. Lora: Low-rank adaptation of large language models. *ICLR*, 1(2):3, 2022. 6
- [19] Rui Huang, Shitong Shao, Zikai Zhou, Pukun Zhao, Hangyu Guo, Tian Ye, Lichen Bai, Shuo Yang, and Zeke Xie. Diffusion dataset condensation: Training your diffusion model faster with less data, 2025. 2, 3
- [20] Ziqi Huang, Yinan He, Jiashuo Yu, Fan Zhang, Chenyang Si, Yuming Jiang, Yuanhan Zhang, Tianxing Wu, Qingyang Jin, Nattapol Chanpaisit, et al. Vbench: Comprehensive benchmark suite for video generative models. In *Proceedings of the IEEE/CVF Conference on Computer Vision and Pattern Recognition*, pages 21807–21818, 2024. 6
- [21] Jin-Young Kim, Hyojun Go, Soonwoo Kwon, and Hyun-Gyoon Kim. Denoising task difficulty-based curriculum for training diffusion models. *arXiv preprint arXiv:2403.10348*, 2024. 3
- [22] Weijie Kong, Qi Tian, Zijian Zhang, Rox Min, Zuozhuo Dai, Jin Zhou, Jiangfeng Xiong, Xin Li, Bo Wu, Jianwei Zhang, et al. Hunyuanvideo: A systematic framework for large video generative models. *arXiv preprint arXiv:2412.03603*, 2024. 1, 2, 3
- [23] Xize Liang, Lin Yang, Jie Wang, Yiyang Lu, Runyu Wu, Hanzhu Chen, and Jianye Hao. Boosting multi-domain fine-tuning of large language models through evolving interactions between samples. In *Forty-second International Conference on Machine Learning*. 3
- [24] Bin Lin, Yunyang Ge, Xinhua Cheng, Zongjian Li, Bin Zhu, Shaodong Wang, Xianyi He, Yang Ye, Shenghai Yuan, Lihuan Chen, et al. Open-sora plan: Open-source large video generation model. *arXiv preprint arXiv:2412.00131*, 2024. 2
- [25] Yaron Lipman, Ricky TQ Chen, Heli Ben-Hamu, Maximilian Nickel, and Matt Le. Flow matching for generative modeling. *arXiv preprint arXiv:2210.02747*, 2022. 2
- [26] Jie Liu, Gongye Liu, Jiajun Liang, Ziyang Yuan, Xiaokun Liu, Mingwu Zheng, Xiele Wu, Qiulin Wang, Menghan Xia, Xintao Wang, et al. Improving video generation with human feedback. *arXiv preprint arXiv:2501.13918*, 2025. 3, 6, 1
- [27] Xiangyang Luo, Xin Zhang, Yifan Xie, Xinyi Tong, Weijiang Yu, Heng Chang, Fei Ma, and Fei Richard Yu. Codeswap: Symmetrically face swapping based on prior codebook. In *Proceedings of the 32nd ACM International Conference on Multimedia*, pages 6910–6919, 2024. 1
- [28] Xiangyang Luo, Junhao Cheng, Yifan Xie, Xin Zhang, Tao Feng, Zhou Liu, Fei Ma, and Fei Yu. Object isolated attention for consistent story visualization. *arXiv preprint arXiv:2503.23353*, 2025. 1

- [29] Xiangyang Luo, Qingyu Li, Xiaokun Liu, Wenyu Qin, Miao Yang, Meng Wang, Pengfei Wan, Di Zhang, Kun Gai, and Shao-Lun Huang. Filmweaver: Weaving consistent multi-shot videos with cache-guided autoregressive diffusion. *arXiv preprint arXiv:2512.11274*, 2025. 1
- [30] Xiangyang Luo, Ye Zhu, Yunfei Liu, Lijian Lin, Cong Wan, Zijian Cai, Yu Li, and Shao-Lun Huang. Canonswap: High-fidelity and consistent video face swapping via canonical space modulation. In *Proceedings of the IEEE/CVF International Conference on Computer Vision*, pages 10064–10074, 2025. 1
- [31] Alexander Quinn Nichol and Prafulla Dhariwal. Improved denoising diffusion probabilistic models. In *International conference on machine learning*, pages 8162–8171. PMLR, 2021. 3
- [32] Mahdi Nikdan, Vincent Cohen-Addad, Dan Alistarh, and Vahab Mirrokni. Efficient data selection at scale via influence distillation. *arXiv preprint arXiv:2505.19051*, 2025. 3
- [33] OpenAI. Sora: Creating video from text. Technical report, OpenAI, 2024. 2
- [34] Robin Rombach, Andreas Blattmann, Dominik Lorenz, Patrick Esser, and Björn Ommer. High-resolution image synthesis with latent diffusion models. In *Proceedings of the IEEE/CVF conference on computer vision and pattern recognition*, pages 10684–10695, 2022. 2
- [35] Christoph Schuhmann, Romain Beaumont, Richard Vencu, Cade Gordon, Ross Wightman, Mehdi Cherti, Theo Coombes, Aarush Katta, Clayton Mullis, Mitchell Wortsman, Patrick Schramowski, Srivatsa Kundurthy, Katherine Crowson, Ludwig Schmidt, Robert Kaczmarczyk, and Jenia Jitsev. Laion-5b: An open large-scale dataset for training next generation image-text models, 2022. 3
- [36] Uriel Singer, Adam Polyak, Thomas Hayes, Xi Yin, Jie An, Songyang Zhang, Qiyuan Hu, Harry Yang, Oron Ashual, Oran Gafni, et al. Make-a-video: Text-to-video generation without text-video data. *arXiv preprint arXiv:2209.14792*, 2022. 2
- [37] Valerii Startsev, Alexander Ustyuzhanin, Alexey Kirillov, Dmitry Baranchuk, and Sergey Kasturylin. Alchemist: Turning public text-to-image data into generative gold. *arXiv preprint arXiv:2505.19297*, 2025. 3
- [38] Cong Wan, Xiangyang Luo, Hao Luo, Zijian Cai, Yiren Song, Yunlong Zhao, Yifan Bai, Fan Wang, Yuhang He, and Yihong Gong. Grid: Omni visual generation. *arXiv preprint arXiv:2412.10718*, 2024. 2
- [39] Team Wan, Ang Wang, Baole Ai, Bin Wen, Chaojie Mao, Chen-Wei Xie, Di Chen, Fei Wu Yu, Haiming Zhao, Jianxiao Yang, et al. Wan: Open and advanced large-scale video generative models. *arXiv preprint arXiv:2503.20314*, 2025. 1, 2, 3, 6
- [40] Bin Xu Wang and John J Vastola. Diffusion models generate images like painters: an analytical theory of outline first, details later. *arXiv preprint arXiv:2303.02490*, 2023. 3
- [41] Qiheng Wang, Yukai Shi, Jiarong Ou, Rui Chen, Ke Lin, Jiahao Wang, Boyuan Jiang, Haotian Yang, Mingwu Zheng, Xin Tao, et al. Koala-36m: A large-scale video dataset improving consistency between fine-grained conditions and video content. In *Proceedings of the Computer Vision and Pattern Recognition Conference*, pages 8428–8437, 2025. 2, 3
- [42] Weijia Wu, Zeyu Zhu, and Mike Zheng Shou. Automated movie generation via multi-agent cot planning. *arXiv preprint arXiv:2503.07314*, 2025. 1
- [43] Mengzhou Xia, Sadhika Malladi, Suchin Gururangan, Sanjeev Arora, and Danqi Chen. Less: Selecting influential data for targeted instruction tuning. *arXiv preprint arXiv:2402.04333*, 2024. 3
- [44] Haiwei Xue, Xiangyang Luo, Zhanghao Hu, Xin Zhang, Xunzhi Xiang, Yuqin Dai, Jianzhuang Liu, Zhensong Zhang, Minglei Li, Jian Yang, et al. Human motion video generation: A survey. *IEEE Transactions on Pattern Analysis and Machine Intelligence*, 2025. 1
- [45] Yongjin Yang, Sihyeon Kim, Hojung Jung, Sangmin Bae, Sangmook Kim, Se-Young Yun, and Kimin Lee. Automated filtering of human feedback data for aligning text-to-image diffusion models, 2024. 3
- [46] Zhuoyi Yang, Jiayan Teng, Wendi Zheng, Ming Ding, Shiyu Huang, Jiazheng Xu, Yuanming Yang, Wenyi Hong, Xiaohan Zhang, Guanyu Feng, et al. Cogvideox: Text-to-video diffusion models with an expert transformer. *arXiv preprint arXiv:2408.06072*, 2024. 2, 6